

Anomalous momentum dependence of the multiband electronic structure of $\text{FeSe}_{1-x}\text{Te}_x$ superconductors induced by atomic disorder

Takaaki Sudayama,¹ Yuki Wakisaka,¹ Daiki Ootsuki,¹ Takashi Mizokawa,^{2,1} Naurang L. Saini,^{3,2} Masashi Arita,⁴ Hirofumi Namatame,⁴ Masaki Taniguchi,^{4,5} Takashi Noji,⁶ and Yoji Koike⁶

¹*Department of Physics, University of Tokyo, 5-1-5 Kashiwanoha, Kashiwa, Chiba 277-8561, Japan*

²*Department of Complexity Science and Engineering, University of Tokyo, 5-1-5 Kashiwanoha, Kashiwa, Chiba 277-8561, Japan*

³*Department of Physics, Università di Roma "La Sapienza", Piazzale Aldo Moro 2, 00185 Roma, Italy*

⁴*Hiroshima Synchrotron Radiation Center, Hiroshima University, Higashihiroshima, Hiroshima 739-0046, Japan*

⁵*Graduate School of Science, Hiroshima University, Higashihiroshima, Hiroshima 739-8526, Japan*

⁶*Department of Applied Physics, Tohoku University, Sendai 980-8579, Japan*

(Dated: August 26, 2021)

When periodicity of crystal is disturbed by atomic disorder, its electronic state becomes inhomogeneous and band dispersion is obscured. In case of Fe-based superconductors, disorder of chalcogen/pnictogen height causes disorder of Fe 3d level splitting. Here, we report an angle-resolved photoemission spectroscopy study on $\text{FeSe}_{1-x}\text{Te}_x$ with the chalcogen height disorder, showing that the disorder affects the Fe 3d band dispersions in an orbital-selective way instead of simple obscuring effect. The reverse of the Fe 3d level splitting due to the chalcogen height difference causes the splitting of the hole band with Fe 3d $x^2 - y^2$ character around the Γ point.

PACS numbers: 74.25.Jb, 74.70.Xa, 79.60.-i, 74.81.-g

The inhomogeneous distributions of spin, charge, lattice, and gap magnitude discovered in high- T_c cuprates¹⁻³ have inspired tremendous research activities on the relationship between the inhomogeneity and the high- T_c superconductivity. The inhomogeneous electronic state is deeply related to the phase competition or the quantum critical phenomenon which plays a central role for the emergence of high- T_c superconductivity. On the other hand, the discoveries of high- T_c superconductivity in Fe pnictides and chalcogenides have created a new wave of research activities on the high- T_c superconductors.⁴ The Fe-based superconductors are based on a multi-orbital system in which several Fermi surfaces with different Fe 3d orbital character are responsible for the superconductivity while the cuprate basically has single Fermi surface mainly derived by the Cu 3d $x^2 - y^2$ orbital. Therefore, although the competition between the magnetism and superconductivity is commonly seen in the cuprates and the Fe pnictides/chalcogenides, the inhomogeneity discovered in the Fe pnictides/chalcogenides could be different from that in the cuprates due to the multi-orbital character.

α -FeSe has the simplest crystal structure (anti-PbO type structure) among the Fe-based superconductors as displayed in Figs. 1(a) and (b)]. While α -FeSe shows superconductivity with $T_c \sim 8$ K,⁵ α -FeTe is not superconducting and, instead, shows incommensurate spin density wave accompanied by structural transition from tetragonal to orthorhombic phase.⁶ The spin density wave of FeTe exhibits a stripe-type spin modulation, the direction of which is different from that of the FeAs-based parent compounds such as LaFeAsO and BaFe₂As₂. $\text{FeSe}_{1-x}\text{Te}_x$ ($0 < x < 0.7$) shows superconductivity with a maximum $T_c \sim 15$ K. An extended x-ray absorption fine-structure (EXAFS) study has revealed that the Se and Te atoms

are distributed with short Fe-Se bonds and long Fe-Te bonds as shown in Fig. 1(b).⁷ Since the difference in chalcogen height between FeSe and FeTe reverses Fe 3d orbital levels as displayed in Figs. 1(c) and (d), the Fe-Se/Te bond disorder may result in the Fe 3d orbital disorder in the real space. In this paper, we report an angle-resolved photoemission spectroscopy (ARPES) study on $\text{FeSe}_{1-x}\text{Te}_x$ which reveal the impact of ligand field reverse between FeSe and FeTe on the fundamental electronic structure of $\text{FeSe}_{1-x}\text{Te}_x$. In $\text{FeSe}_{1-x}\text{Te}_x$, the distribution of the Fe-Se and Fe-Te bonds in the real space causes the splitting of the hole band with Fe 3d $x^2 - y^2$ character around the Γ point in the momentum space. Since the hole pocket of the Fe 3d $x^2 - y^2$ band is expected to play important roles in various proposed pairing mechanisms including s_{+-} pairing by spin fluctuation^{8,9} and s_{++} pairing by orbital fluctuation,¹⁰ the present study on the orbital-selective band splitting due to the chalcogen height disorder suggests that the inhomogeneity in the orbital channel should be included to describe the Fe-based superconductors.

We have studied single crystals of annealed $\text{FeSe}_{1-x}\text{Te}_x$ with $x = 0.6$ and 0.9 which were grown as reported by Noji *et al.*¹¹ ARPES measurements were performed at beamline 9A, Hiroshima Synchrotron Radiation Center (HSRC) which has a normal incidence monochromator with off-plane Eagle mounting. The end station is equipped with a SCIENTA R4000 analyzer for angle-resolved photoemission experiments, which is a 200 mm mean radius spectrometer. The helical undulator and the monochromator provides circularly polarized light for the energy range of 4-30 eV. In the present experiment, the photon energy was set to $h\nu = 17$ eV and 23 eV. Total energy resolutions including the monochromator and the electron analyzer were set to 18

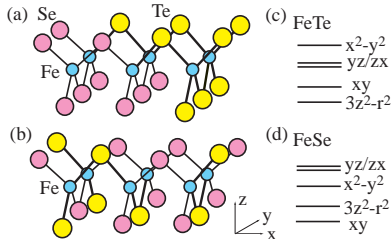


FIG. 1: (Color online) (a) Crystal structure of FeSe/FeTe and (b) that of $\text{FeSe}_{1-x}\text{Te}_x$ with short Fe-Se bonds and long Fe-Te bonds. The FeTe_4 tetrahedron is elongated along the z -axis compared to the FeSe_4 tetrahedron. (c) Fe 3d energy levels for FeTe and (d) those for FeSe.

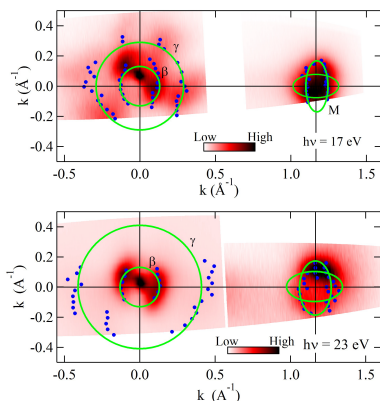


FIG. 2: (Color online) Fermi surface mappings for annealed $\text{FeSe}_{0.4}\text{Te}_{0.6}$ at $h\nu = 17$ eV and $h\nu = 23$ eV. The dots indicate the band locations determined by peak positions of second derivative of MDC.

meV and 14 meV for $h\nu = 23$ eV and 17 eV, respectively. The base pressure of the spectrometer was 10^{-9} Pa range. The single crystals were properly oriented on the sample stage by the standard Laue measurements and were cooled using liquid He refrigerator. We cleaved the single crystals at 14 K under ultrahigh vacuum and took ARPES data at 14 K within four hours after the cleavage.

Figure 2 shows Fermi surfaces of annealed $\text{FeSe}_{1-x}\text{Te}_x$ with $x = 0.6$ taken at $h\nu = 17$ eV and 23 eV. For the Fermi surface mapping, we used ARPES intensity integrated within an energy window of ± 5 meV at the Fermi level (E_F). The momentum points where the bands cross E_F can be determined by maximum points in second derivative spectrum of momentum distribution curve (MDC) at E_F . The momentum points thus determined are indicated by the dots, and the Fermi surfaces deduced from the dots are shown in the maps. The cut from Γ (zone center) to M (zone corner) corresponds to the in-plane Fe-Fe direction. As commonly observed in various

Fe-based superconductors, the hole-like Fermi surfaces around Γ and the electron-like Fermi surface around M are observed. The area of the outer Fermi surface increases in going from $h\nu = 17$ eV to $h\nu = 23$ eV, indicating that the Fermi surface depends on the momentum perpendicular to the FeSe plane. In the following discussion, we focus on the ARPES data taken at $h\nu = 23$ eV in which the Γ point (zone center) of the two-dimensional Brillouin zone is rather close the Z point of the three-dimensional Brillouin zone, and the hole bands are more clearly observed compared to those at $h\nu = 17$ eV.

Figure 3(a) shows band dispersions along the Γ -M direction of annealed $\text{FeSe}_{1-x}\text{Te}_x$ with $x = 0.6$ at $h\nu = 23$ eV. The band dispersions are extracted from the EDC data displayed in Fig. 3(b). Three hole-like bands at the zone center are clearly observed. Among them, two outer hole-like bands cross E_F and the inner hole-like band does not cross E_F with top position at about 20 meV below E_F judging from the energy distribution curve (EDC). (It is very difficult to identify the band top using the second derivative spectrum of MDC since the tail above the band top, which is mainly due to finite energy resolution, appears as a maximum point in MDC.) This is consistent with two hole-like pockets around the zone center (Γ point) observed in Fig. 2, and is qualitatively consistent with the previous ARPES results on $\text{FeSe}_{0.42}\text{Te}_{0.58}$,¹² FeTe ,¹³ $\text{Fe}_{1.03}\text{Te}_{0.7}\text{Se}_{0.3}$,¹⁴ and $\text{FeSe}_{0.5}\text{Te}_{0.5}$.¹⁵

The present results show that the effect of Fe-Se/Te bond disorder is apparently small in the momentum space. The difference of Fe-Se/Te bond, in particular, Se/Te height from the Fe plane is predicted to give substantial change of the electronic structure between FeSe and FeTe both in the zone center and zone corner.¹² In the case of FeSe, there are the $x^2 - y^2$ band below E_F and only yz/zx bands crossing E_F around Γ point, while, in the case of FeTe, there are three bands crossing E_F and $x^2 - y^2$ (yz/zx) bands have higher (lower) energy around Γ . Although the Fe 3d orbitals are completely disordered due to the bond disorder, the clear band structures survive around the zone center. Here, it should be noted that the Se/Te distribution in $\text{FeSe}_{1-x}\text{Te}_x$ becomes more homogeneous or more random by annealing as confirmed by x-ray diffraction analysis and electron probe micro analysis.^{16,17}

The momentum dependent effect of atomic disorder in random alloys of $AB_{1-x}C_x$,¹⁸ in which the local structure around the A site is disordered although the end members AB and AC possessing perfect crystallographic symmetry,¹⁹ provides a hint to understand the ARPES results of $\text{FeSe}_{0.4}\text{Te}_{0.6}$. In the strongly perturbed alloys, the band structure of $AB_{1-x}C_x$ deviates from the average between those of AB and AC due to formation of impurity bands. The specialty of Fe(Se,Te) is that the Fe 3d level splitting is reversed between FeSe and FeTe. The EXAFS results⁷ indicate that the Fe 3d orbital splitting locally have FeSe-like orbital state or FeTe-like orbital state instead of the average between them. In such case,

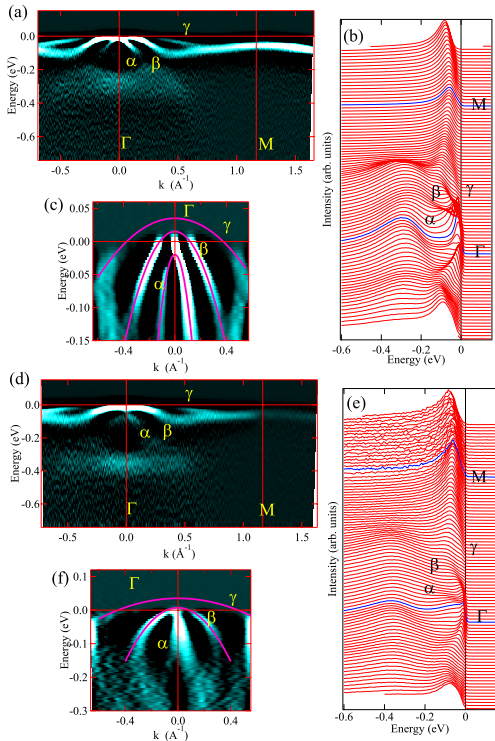


FIG. 3: (Color online) ARPES results for annealed $\text{FeSe}_{0.4}\text{Te}_{0.6}$ taken at $h\nu = 23$ eV. (a) Second derivative plot of EDC. (b) EDC spectrum along Γ -M. (c) Second derivative plot of MDC around Γ point. ARPES results for annealed $\text{FeSe}_{0.1}\text{Te}_{0.9}$ taken at $h\nu = 23$ eV. (d) Second derivative plot of EDC. (e) EDC spectrum along Γ -M. (f) Second derivative plot of MDC around Γ point.

the FeSe-like band dispersion and the FeTe-like band dispersion can coexist in the momentum space to be observed by ARPES.

In order to support this scenario on the coexistence of FeSe-like and FeTe-like band dispersions, momentum distribution of single-electron excitation is calculated using a 19-site one-dimensional (1D) model and a 19×19 -sites two-dimensional (2D) model with random Fe $3d$ level splitting. In the present models with Fe $3d$ $x^2 - y^2$, yz , and zx orbitals, the energies of $x^2 - y^2$, yz , and zx are set to $-2t$ ($2t$), 0 , 0 at the FeSe-like (FeTe-like) sites to consider the reverse of orbital splitting. In the 1D model with lattice constant a , the transfer integrals between the neighboring $x^2 - y^2$ and zx orbitals are set to t while those between the neighboring yz orbitals are set to $t/2$. In the 2D square lattice model with lattice constant a , the transfer integrals between the neighboring xy orbitals are $t/2$ along the x - and y -axes and those between the neighboring yz (zx) orbitals are $t/4$ and $t/2$ ($t/2$ and $t/4$) along the x - and y -axes respectively. All the configurations for $\sim 40\%$ FeSe-like sites and $\sim 60\%$ FeTe-like sites are included in the 1D case while 10000 configurations are randomly selected for the 2D case. The calculated momentum distribution for the 1D model is displayed in Fig.

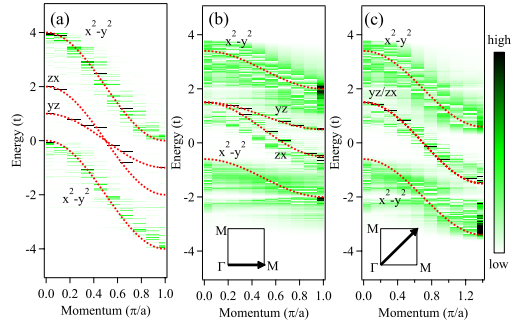


FIG. 4: (Color online) Momentum distribution of single-electron excitation (a) for the 1D multi-band model with random orbital level splitting, (b) for the $(0,0)$ to $(\pi,0)$ direction of 2D model, (c) for the $(0,0)$ to (π,π) direction of 2D model. Momentum and energy are given in units of π/a and t where a is the lattice constant and t is the transfer integral.

4(a) where the Fe $3d$ $x^2 - y^2$ band is split into the two bands which correspond to the FeTe-like and FeSe-like band dispersions (roughly follow $\epsilon_k = \pm 2t + 2t \cos(k_x)$ as indicated by the dotted curves respectively). The splitting of the Fe $3d$ band is also reproduced in the 2D model along the $(0,0)$ to $(\pi/a,0)$ direction [Fig. 4(b)] and along the $(0,0)$ to $(\pi/a,\pi/a)$ direction [Fig. 4(c)]. In the 2D case, the band dispersions of the Fe $3d$ $x^2 - y^2$ bands are roughly fit to $\epsilon_k = \pm 2t + 0.7t[\cos(k_x) + \cos(k_y)]$ (shown by the dotted curves) indicating that renormalization effect with factor of 0.7. The renormalization effect due to the random orbital distribution could contribute to the enhancement of electronic specific heat in $\text{FeSe}_x\text{Te}_{1-x}$.

The ARPES results of $\text{FeSe}_{0.4}\text{Te}_{0.6}$ can be interpreted on the basis of the present calculations. The inner hole band labeled as α can be assigned to the $x^2 - y^2$ band of the FeSe-like orbital state. On the other hand, the outer hole band labeled as γ is derived from the $x^2 - y^2$ band of the FeTe-like orbital state. The yz/zx bands of FeSe- and FeTe-like orbital states, which are almost degenerate in the LDA calculations,¹² can be merged as demonstrated in the above calculations and can be observed as β . At $x = 0.6$, the annealing induces small increase of T_c ¹¹ which is probably due to strain relaxing

atomic redistribution for the two kinds of orbital states, suppressing the magnetic order of FeTe-like orbital domains (compressive for the one and tensile for the other domains) as happens in various granular superconductors and random alloys.¹⁸ At this point, it is very interesting and important to study $x = 0.9$ in which the as-grown sample is not superconducting and the annealing induces $T_c \sim 11$ K.¹¹

Figure 3(d) shows band dispersions of annealed $\text{FeSe}_{1-x}\text{Te}_x$ with $x = 0.9$ at $h\nu = 23$ eV. The band dispersions are extracted from the EDC data displayed in Figs. 3(e). At least two hole-like bands at the zone center are observed. The Te rich sample is dominated by the FeTe-like orbital states. Therefore, it is expected that the $x^2 - y^2$ band (labeled as γ) is higher in energy than the yz/zx band at the zone center and the $x^2 - y^2$ band is smoothly connected to the flat band at the zone corner. This expectation is consistent with the observed band dispersions shown in Figs. 3(d) and (f). In addition, the width of the outer hole band labeled as γ is smaller at $x = 0.9$ than $x = 0.6$. Such band structure of FeTe is known to support magnetic state instead of superconductivity. However, at $x = 0.9$, the Se/Te distribution helps to form FeSe-like orbital site where the yz/zx band (labeled as β) is higher in energy than the $x^2 - y^2$ band (labeled as

α). Here, it should be noted that the intensity of band α is very small at $x = 0.9$ compared to that at $x = 0.6$, consistent with the assumption that it is derived from the minor FeSe-like orbital state. At this stage, one can speculate that the superconductivity appears at $x = 0.9$ due to strain relaxing distribution of the domains with different orbital states on annealing.

In conclusion, we have reported an ARPES study on the annealed $\text{FeSe}_{1-x}\text{Te}_x$ ($x = 0.6$ and 0.9). The comparison between the band dispersions at $x = 0.6$ and those at $x = 0.9$ shows that the disorder of Fe $3d$ level splitting affects the Fe $3d$ band dispersions in an orbital-selective way. The hole bands at the zone center in $\text{FeSe}_{1-x}\text{Te}_x$ can be assigned to the Fe $3d$ bands from the FeSe-like and the FeTe-like orbital states as supported by the model calculation. At $x = 0.9$, the minor FeSe-like orbital state may induce the superconductivity due to strain relaxing atomic distribution under the atomic disorder.

The synthesis and characterization of the $\text{FeSe}_{1-x}\text{Te}_x$ single crystals were supported by a Grant-in-Aid for Scientific Research from the Japan Society for Promotion of Science. The synchrotron radiation experiments have been done with the approval of HSRC (Proposal No. 10-A-10).

-
- ¹ J. M. Tranquada, B. J. Sternlieb, J. D. Axe, Y. Nakamura, S. Uchida, *Nature* **375**, 561 (1995).
- ² A. Bianconi, N. L. Saini, A. Lanzara, M. Missori, T. Rossetti, H. Oyanagi, H. Yamaguchi, K. Oka, T. Ito, *Phys. Rev. Lett.* **76**, 3412 (1996).
- ³ K. M. Lang, V. Madhavan, J. E. Hoffman, E. W. Hudson, H. Eisaki, S. Uchida, *Nature* **415**, 412 (2002).
- ⁴ Y. Kamihara, T. Watanabe, M. Hirano, and H. Hosono, *J. Am. Chem. Soc.* **130**, 3296 (2008).
- ⁵ F. C. Hsu, J. Y. Luo, K. W. The, T. K. Chen, T. W. Huang, P. M. Wu, Y. C., Lee, Y. L. Huang, Y. Y. Chu, D. C. Yan, M. K. Wu, *Proc. Natl. Acad. Sci. U.S.A.* **105**, 14262 (2008).
- ⁶ W. Bao, Y. Qiu, Q. Huang, M. A. Green, P. Zajdel, M. R. Fitzsimmons, M. Zhernenkov, S. Chang, M. Fang, B. Qian, E. K. Vehstedt, J. Yang, H. M. Pham, L. Spinu, Z. Q. Mao, *Phys. Rev. Lett.* **102**, 247001 (2009).
- ⁷ B. Joseph, A. Iadecola, A. Puri, L. Simonelli, Y. Mizuguchi, Y. Takano, N. L. Saini, *Phys. Rev. B* **82**, 020502 (2010).
- ⁸ K. Kuroki, S. Onari, R. Arita, H. Usui, Y. Tanaka, H. Kontani, and H. Aoki, *Phys. Rev. Lett.* **101**, 087004 (2008).
- ⁹ I. I. Mazin, D. J. Singh, M. D. Johannes, and M. H. Du, *Phys. Rev. Lett.* **101**, 057003 (2008).
- ¹⁰ H. Kontani and S. Onari, *Phys. Rev. Lett.* **104**, 157001 (2010).
- ¹¹ T. Noji, T. Suzuki, H. Abe, T. Adachi, M. Kato, Y. Koike, *J. Phys. Soc. Jpn.* **79**, 084711 (2010).
- ¹² A. Tamai, A. Y. Ganin, E. Rozbicki, J. Bacsá, W. Meevasana, P. D. C. King, M. Caffio, R. Schaub, S. Margadonna, K. Prassides, M. J. Rosseinsky, F. Baumberger, *Phys. Rev. Lett.* **104**, 097002 (2010).
- ¹³ Y. Xia, D. Qian, L. Wray, D. Hsieh, G. F. Chen, J. L. Luo, N. L. Wang, M. Z. Hasan, *Phys. Rev. Lett.* **103**, 037002 (2009).
- ¹⁴ K. Nakayama, T. Sato, P. Richard, T. Kawahara, Y. Sekiba, T. Qian, G. F. Chen, J. L. Luo, N. L. Wang, H. Ding, T. Takahashi, *Phys. Rev. Lett.* **105**, 197001 (2010).
- ¹⁵ S.-H. Lee, G. Xu, W. Ku, J. S. Wen, C. C. Lee, N. Katayama, Z. J. Xu, S. Ji, Z. W. Lin, G. D. Gu, H.-B. Yang, P. D. Johnson, Z.-H. Pan, T. Valla, M. Fujita, T. J. Sato, S. Chang, K. Yamada, J. M. Tranquada, *Phys. Rev. B* **81**, 220502(R) (2010).
- ¹⁶ M. Imaizumi, T. Noji, T. Adachi, Y. Koike, *Physica C* **471**, 614 (2011).
- ¹⁷ T. Taen, Y. Tsuchiya, Y. Nakajima, T. Tamegai, *Phys. Rev. B* **80**, 092502 (2009).
- ¹⁸ V. Popescu and A. Zunger, *Phys. Rev. Lett.* **104**, 236403 (2010).
- ¹⁹ P. F. Peterson, Th. Proffen, I.-K. Jeong, S. J. L. Billinge, K.-S. Choi, M. G. Kanatzidis, P. G. Radaelli, *Phys. Rev. B* **63**, 165211 (2001).